PERGAMON

International Journal of Heat and Mass Transfer 41 (1998) 3719–3729

International Journal of HEAT and MASS TRANSFER

# Evaporative cooling of liquid film in turbulent mixed convection channel flows

Wei-Mon Yan*

*Department of Mechanical Engineering, Huafan University, Shih Ting, Taipei 22305, Taiwan, Republic of China*

Received 15 October 1997; in final form 6 March 1998

**Abstract**

A detailed numerical study has been performed to investigate the evaporative cooling of liquid falling film through interfacial heat and mass transfer in turbulent mixed convection channel flows. The effects of gas–liquid phase coupling, variable thermophysical properties and film vaporization are considered in the analysis. Simultaneous mass, momentum and heat transfer between liquid film and gas stream is numerically studied by solving the respective governing equations for the liquid film and gas stream together. In the gas stream, the low Reynolds number turbulent $k$–$\varepsilon$ model has been used to simulate the turbulent flow. Results are presented for an air–water system under different conditions. Particular attention is paid to investigating the role of latent heat transport associated with the film vaporization. Results show that the heat transfer from the gas–liquid interface to the gas stream is predominantly determined by the latent heat transfer connected with film evaporation. Additionally, better liquid film cooling is noticed for the system having a higher inlet liquid temperature $T_{\ell i}$, a lower liquid flowrate $B$ or a higher gas flow Reynolds number $Re$. 

**Nomenclature**

$b$ half channel width [m]
$B$ liquid mass flow rate per unit periphery length at inlet [kg m$^{-1}$ s$^{-1}$]
$C_1$, $C_2$, $C_\mu$ constants appearing in turbulent $k$–$\varepsilon$ equations
$c_p$ specific heat [J kg$^{-1}$ K$^{-1}$]
$D$ mass diffusivity [m$^2$ s$^{-1}$]
$h_{fg}$ latent heat of vaporization [J kg$^{-1}$]
$f_2$, $f_\mu$ functions appearing in turbulent k–$\varepsilon$ eqns
$g$ gravitational acceleration [m s$^{-2}$]
$h_M$ mass transfer coefficient
$k$ turbulent kinetic energy [m$^2$ s$^{-2}$]
$\dot{m}''_I$ evaporating mass flux [kg s$^{-1}$ m$^{-2}$]
$M_a$ molar mass of air [kg K$^{-1}$ mol$^{-1}$]
$M_v$ molar mass of vapor [kg K$^{-1}$ mol$^{-1}$]
$Nu_\ell$ local Nusselt number for latent heat transport, eqn (18)
$Nu_S$ local Nusselt number for sensible heat transport, eqn (17)
$Nu_x$ overall Nusselt number, eqn (15) ($Nu_S+Nu_\ell$)
$p_I$ partial pressure of water vapor at the gas–liquid interface [kPa]
$Pr_t$ turbulent Prandtl number
$p$ mixture pressure [kPa]
$p_m$ motion pressure, $p-p_0$
$q''_I$ total interfacial energy flux, eqn (14) [W m$^{-2}$]
$q''_{fl}$ latent heat flux (or net enthalpy flux), $\dot{m}''_I \cdot h_{fg}$ [W m$^{-2}$]
$q''_{sI}$ sensible heat flux [W m$^{-2}$]
$Re$ gas stream Reynolds number, $\bar{u}_f \cdot 4b/v_0$
$R_t$ turbulent Reynolds number, $k^2/(v\varepsilon)$
$Sh$ local Sherwood number
$T$ temperature [K] [°C]
$T_{\ell i}$ inlet liquid film temperature [K] [°C]
$T_0$ inlet temperature of the gas stream [K] [°C]
$u$ axial velocity [m s$^{-1}$]
$u_f$ fully-developed velocity at inlet [m s$^{-1}$]
$\bar{u}_f$ average inlet velocity [m s$^{-1}$]
$u_*$ shear stress velocity, $(\tau_W/\rho)^{1/2}$
$v$ transverse velocity [m s$^{-1}$]
$w$ mass fraction of water vapor
$x$ coordinate in the flow direction [m]
$X$ dimensionless axial location, $x/b$

* Tel.: 00886 2 26632102 ext. 4038; fax: 00 886 2 26631119; e-mail: wmyan@huafan.hfu.edu.tw

0017–9310/98 $19.00 
PII: S0017–9310(98)00105–7

$y$ coordinate in the transverse direction [m]
$y^+$ dimensionless wall coordinate, $(b-y-\delta)\cdot u_*/v$.

*Greek symbols*
$\alpha$ thermal diffusivity [$m^2\ s^{-1}$]
$\beta$ coefficient of thermal expansion
$\delta$ local liquid film thickness [m]
$\varepsilon$ the rate of dissipation of turbulent kinetic energy [$m^2\ s^{-3}$]
$\lambda$ molecular thermal conductivity [$W\ m^{-1}\cdot{}^\circ C$]
$\lambda_t$ turbulent eddy conductivity [$W\ m^{-1}\cdot{}^\circ C$]
$\tau$ shear stress [kPa]
$\mu$ molecular dynamic viscosity [$N\cdot s\ m^{-2}$]
$\mu_t$ turbulent eddy viscosity [$N\cdot s\ m^{-2}$]
$\rho$ density [$kg\ m^{-3}$]
$\phi$ relative humidity at inlet
$\sigma_k$ turbulent Prandtl number for $k$
$\sigma_\varepsilon$ turbulent Prandtl number for $\varepsilon$.

*Subscripts*
a of air
b bulk quantity
g mixture (air + water vapor)
I condition at gas–liquid interface
$\ell$ liquid film
o condition at inlet
t turbulent
v of vapor
w condition at wall.

## 1. Introduction

The simultaneous heat and mass transfer between a liquid film and binary mixture is encountered in many engineering applications, such as in an air cooler, condenser, evaporator, cooling tower, drying process and a heat recovery process from waste heat water. Due to their widespread applications, heat and mass transfer between flowing hot liquid film and a cold air stream has received considerable attention. Whereas a large number of investigations have been made concerning the heat and mass transfer problems, the study of the evaporative cooling of liquid film in turbulent mixed channel flows has not received adequate attention.

The aiding–buoyancy force on turbulent forced convection heat transfer in a vertical pipe was examined by Carr et al. [1], Connor and Carr [2] and Ackerman [3]. Their results showed that at high Grashof numbers a limiting profile shape was approached, with maximum velocity shifting toward the heated wall. Additionally, it is found that the heat transfer from the wall is impaired in the low ranges of the Grashof numbers, but recovers and may even exceed the pure forced-convection value at high Grashof numbers. For turbulent mixed convection in buoyancy-opposed flow in vertical tubes, the heat transfer is generally enhanced over that for pure forced convection [4, 5]. Turbulent mixed convection between vertical parallel plates subjected to different wall temperatures was investigated by Nakajima et al. [6]. In order to simulate the problem, they adopted a modified mixing length model to examine the effects of aiding and opposing buoyancy forces on fully-developed turbulent forced convection. By employing the modified turbulent $k$–$\varepsilon$ model, Abdelmeguid and Spalding [7], Tanaka et al. [8], Cotton and Jackson [9] and Torii et al. [10] successfully predicted the turbulent mixed convection flow and heat transfer in vertical tubes.

The detailed analysis of the transfer processes between the gas stream mixture and liquid film is inherently complex due to the nonlinear couplings between the momentum, heat and mass transfer in the flow. Hence, the early studies mainly focused on heat and mass transfer in the gas stream by assuming the liquid film to be extremely thin. Under this assumption the transport in the liquid film can be replaced by the approximate boundary conditions for the gas flow. This type of analysis was carried out for forced convection heat and mass transfer over a flat plate [11–13] and a wedge [14]. A similar study was conducted by Chandra and Savery [15] and Chandra [16] for an upward forced air over a falling isopropyl alcohol film by the integral method. In their theoretical work the measured temperature and concentration distributions along the gas–liquid interface were used to specify the nonhomogenous boundary conditions for solving the energy and concentration equations for the air–vapor flow. As far as mixed convection heat and mass transfer is concerned, Yan and his colleagues [17–20] numerically investigated the laminar or turbulent mixed convection flow in vertical ducts under the simultaneous influence of the combined buoyancy forces of thermal and mass diffusion. However, their results are limited by the assumption that the liquid film on the wetted wall is negligibly thin.

Heat and mass transfer in vertical tubes with consideration of transport processes in liquid film was numerically examined by Baumann and Thiele [21, 22]. In these studies, a linear temperature distribution across the film was assumed. Additionally, the buoyancy effects were ignored. The evaporative cooling of liquid falling film in natural convection channel flows was explored by Yan and his colleagues [23, 24]. The results show that the evaporative cooling of liquid film in natural convection channel flows is mainly caused by the latent heat transport connected with film evaporation. Often, in practical applications, the turbulent forced gas stream over a vaporizing liquid film is encountered. This motivates the present study which examines the evaporative cooling of liquid film in a turbulent channel flow with thermal and solutal buoyancy effects.

## 2. Analysis

Partial filmwise evaporation of air–water mixtures is considered in a vertical channel with concurrent downstream flow of both the gas stream and the falling liquid film (see Fig. 1). The thin liquid film is fed with an inlet liquid temperature $T_{\ell i}$ and inlet liquid mass flow rate $B$. The falling liquid film along the channel wall satisfies no slip condition. The channel walls are thermally insulated in order to investigate the evaporative cooling of liquid film, associated with the latent heat transport of film vaporization. The flow of moist air with relative humidity $\phi$ enters the channel from the top end with a fully-developed velocity $u_f$ and uniform temperature $T_0$ and concentration $w_0$. The interfacial heat and mass transfer is apparently determined by the coupled transport processes in the liquid film and gas stream. The liquid film evaporates into the gas stream as it flows downstream, and thus generates thermal and solutal buoyancy forces. Therefore, the turbulent forced gas flow is modified by these buoyancy forces along with the shearing effect created by the falling film.

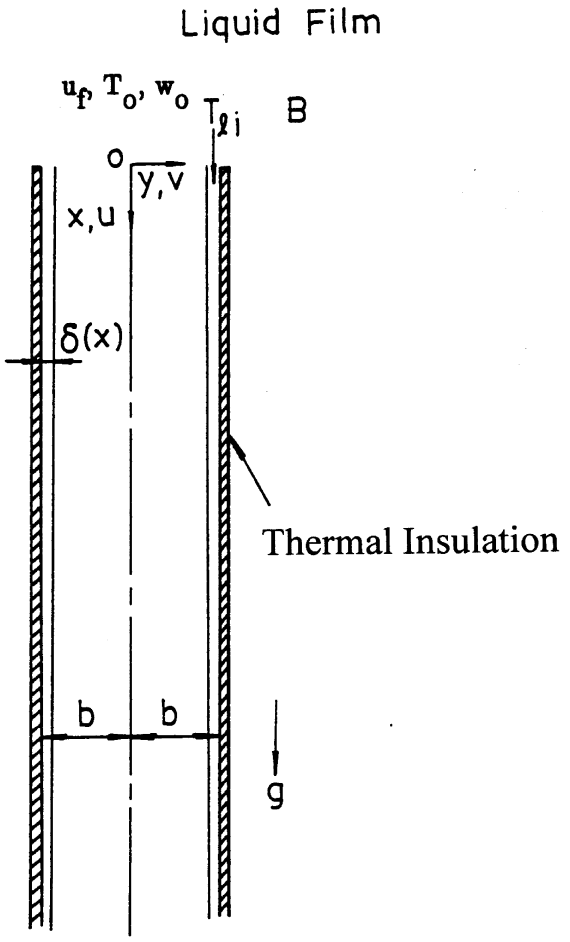


Fig. 1. Schematical diagram of the physical system.

### 2.1. Basic equations for liquid film

As shown in the studies of Dukler [25] and Kafesjan et al. [26], the surface waves on a falling liquid film at $Re_\ell > 16$ normally appear except in the region near the start of the flow. The waves are of three-dimensional and unsteady characteristics. Due to the complexity of the wave motion, an assumption of the time-wise steady film thickness used in numerous investigations [27, 28] is adopted in the present study. This steady film thickness can be interpreted as the temporal average of the large amplitude waves on the surface of the actual film [27]. Additionally, to facilitate the analysis, the inertia terms in the liquid–film momentum equation are neglected as compared with the diffusion term [21, 22]. Therefore, the two-dimensional boundary layer flow in the liquid film is governed by the axial momentum and energy equations as follows:

axial momentum equation

$$0 = \partial(\mu_\ell \partial u_\ell/\partial y)/\partial y + \rho_\ell g \tag{1}$$

energy equation

$$\rho_\ell c_{p\ell} u_\ell \partial T_\ell/\partial x = \partial(\lambda_\ell \partial T_\ell/\partial y)/\partial y \tag{2}$$

### 2.2. Basic equations for gas stream

Steady convection heat and mass transfer in a turbulent gas stream can be explored, with the usual boundary layer approximations, by the following equations:

continuity

$$\partial(\rho u)/\partial x + \partial(\rho v)/\partial y = 0 \tag{3}$$

axial momentum equation

$$\rho u \partial u/\partial x + \rho v \partial u/\partial y = -\mathrm{d}p_m/\mathrm{d}x + \partial[(\mu+\mu_t)\partial u/\partial y]/\partial y - (\rho_0 - \rho)g \tag{4}$$

energy equation

$$\rho c_p u \partial T/\partial x + \rho c_p v \partial T/\partial y = \partial[(\lambda+\lambda_t)\partial T/\partial y]/\partial y \tag{5}$$

concentration equation of water vapor

$$\rho u \partial w/\partial x + \rho v \partial w/\partial y = \partial[\rho(D+D_t)\partial w/\partial y]/\partial y \tag{6}$$

where $\mu_t$, $\lambda_t$, and $D_t$ denote the turbulent viscosity, conductivity and mass diffusivity of the gas mixture, respectively. It is noted in eqn (4) that the third term on the right hand side represents the buoyancy forces due to the variations in temperature and concentration.

In the study of steady channel flow, the following equation of overall mass balance at every axial location is used to reduce the pressure gradient in the gas flow.

$$\int_0^{b-\delta} \rho_g u \,\mathrm{d}y = \rho_0 \bar{u}_f (b-\delta_0) - \int_0^x \rho_g v_I \,\mathrm{d}x \tag{7}$$

### 2.3. Boundary and interfacial conditions

The two sets of governing equations, eqns (1)–(6), are subjected to the following boundary conditions: at the channel wall the no-slip conditions for $u$- and $v$-velocities have to be satisfied as well as an insulated wall condition. On the channel axis all gradients in the mixture flow will be zero because of symmetry arguments. The inlet conditions are fully-developed velocity and flat temperature and concentration distributions.

The interfacial matching conditions specified at the gas–liquid interface, $y = b-\delta(x)$, are described as follows:

(1) Continuities of velocity and temperature

$$u_I(x) = u_{g,I} = u_{\ell,I}, T_I(x) = T_{g,I} = T_{\ell,I} \tag{8}$$

(2) Continuity of shear stress

$$\tau_I(x) = [(\mu+\mu_t)\cdot(\partial u/\partial y)]_{g,I} = (\mu\partial u/\partial y)_{\ell,I} \tag{9}$$

(3) Transverse velocity of the air–vapor mixture is deduced by assuming the interface is semipermeable [29], that is, the solubility of air in the liquid film is negligibly small and the $y$-component of air velocity is zero at the interface

$$v_I = [(D+D_t)/(1-w_I)]\cdot(\partial w/\partial y)_I \tag{10}$$

(4) By assuming the interface to be in thermodynamic equilibrium and the air–vapor mixture an ideal gas mixture, the mass fraction of the vapor can be evaluated by [29]

$$w_I = M_v p_I/[M_a(p-p_I)+M_v p_I] \tag{11}$$

where $p_I$ is the partial pressure of the vapor at the gas–liquid interface. $M_v$ and $M_a$ denote the molar mass of the water vapor and air, respectively.

(5) Vaporizing flux of water vapor into the gas flow

$$\dot{m}_I'' = -\rho v_I = \rho(D+D_t)/(1-w_I)\cdot\partial w/\partial y \tag{12}$$

(6) Energy balance at the gas–liquid interface

$$(\lambda\partial T/\partial y)_{\ell,I} = [(\lambda+\lambda_t)\cdot(\partial T/\partial y)]_{g,I}+\dot{m}_I''\cdot h_{fg} \tag{13}$$

Equation (13) states that at the interface the energy can be transported into the gas stream in two modes. One is the sensible heat transfer via the gas temperature gradient, $q_{sI}''$. The other is through the latent heat transfer via the liquid film vaporization, $q_{\Pi}''$. Therefore, the total interfacial heat transfer from the liquid to the gas stream, $q_I''$, can be expressed as

$$q_I'' = q_{sI}''+q_{\Pi}'' = [(\lambda+\lambda_t)\cdot(\partial T/\partial y)]_{g,I}+\dot{m}_I''\cdot h_{fg} \tag{14}$$

The local Nusselt number along the gas–liquid interface, defined as

$$Nu_x = h\cdot(4b)/\lambda_g = q_I''\cdot(4b)/[\lambda_g\cdot(T_I-T_b)] \tag{15}$$

can be written as

$$Nu_x = Nu_s+Nu_\ell \tag{16}$$

where $Nu_s$ and $Nu_\ell$ are the local Nusselt numbers for sensible and latent heat transfer, respectively, and are evaluated by

$$Nu_s = q_{sI}''\cdot(4b)/[\lambda_g(T_I-T_b)] \tag{17}$$

and

$$Nu_\ell = q_{\Pi}''\cdot(4b)/[\lambda_g(T_I-T_b)] \tag{18}$$

Similarly, the local Sherwood number at the interface is defined as

$$Sh = h_M\cdot(4b)/D = \dot{m}_I''\cdot(1-w_I)\cdot(4b)/[\rho_g D(w_I-w_b)] \tag{19}$$

Note that in the above formulation the thermophysical properties of the gas mixture and liquid film are considered as variable with temperature and mixture composition. They are calculated from the pure component data by means of mixing rules [30, 31] applicable to any multicomponent mixtures. The pure component data [32] are approximated by polynomials in terms of temperature.

## 3. Turbulence modeling

For simulation of turbulence in the gas flow, a modified low Reynolds number k–ε model developed by Myong et al. [33] and Myong and Kasagi [34] is adopted to eliminate the usage of wall functions in the computation and thus to permit direct integration of the transport equations to the gas–liquid interface. The equations of the modified low–Reynolds number $k$–$\varepsilon$ model are as follows:

the turbulent kinetic energy equation

$$\rho u\partial k/\partial x+\rho v\partial k/\partial y = \partial[(\mu+\mu_t/\sigma_k)\partial k/\partial y]/\partial y+\mu_t(\partial u/\partial y)^2-\rho\varepsilon \tag{20}$$

the rate of dissipation of turbulent kinetic energy equation

$$\rho u\partial\varepsilon/\partial x+\rho v\partial\varepsilon/\partial y = \partial[(\mu+\mu_t/\sigma_\varepsilon)\partial\varepsilon/\partial y]/\partial y+C_1(\varepsilon/k)\mu_t(\partial u/\partial y)^2-\rho C_2 f_2\varepsilon^2/k \tag{21}$$

where

$$\mu_t = \rho C_\mu f_\mu k^2/\varepsilon \tag{22}$$

$$f_2 = \{1-(2/9)\exp[-(R_t/6)^2]\}[1-\exp(-y^+/5)]^2 \tag{23}$$

$$f_\mu = (1+3.45/\sqrt{R_t})\cdot[1-\exp(-y^+/70)] \tag{24}$$

$$R_t = k^2/(v\varepsilon), y^+ = (b-y-\delta)u_*/v, u_* = (\tau_w/\rho)^{1/2} \tag{25}$$

The other empirical constants take the following values [33, 34]:

$$\sigma_k = 1.4, \sigma_\varepsilon = 1.3, C_1 = 1.4, C_2 = 1.8, C_\mu = 0.09 \quad (26)$$

## 4. Solution method

Due to the interactions between the liquid film and the gas stream, through their common interfaces, the solution for the problem can be better sought by finite difference procedures. Since the flow under consideration is of a boundary–layer type, the finite difference solution for eqns (1)–(6) are in the downstream direction. The governing equations are expressed in terms of finite difference approximations by employing the upstream difference in the axial convection terms and the central difference in the transverse convection and diffusion terms. The resulting system of algebraic equations can be cast into a tridiagonal matrix equation, which can be efficiently solved by the TDMA method [35]. In the present study the matching conditions imposed at the gas–liquid interface, eqns (9) and (13), are cast in backward difference for $(\partial\psi/\partial y)_g$ and forward difference for $(\partial\psi/\partial y)_\ell$ with $\psi$ denoting $u$ to $T$. Therefore, the governing equations in the gas flow and liquid film can be solved simultaneously.

To obtain enhanced accuracy in numerical computations, grids are nonuniformly distributed in both axial and transverse directions to account for the uneven variations of $u$, $T$ and $w$. The grids are transversely clustered near the gas–liquid interface, and the grid density is also higher in the region near the inlet. The transverse distribution of grid nodes is arranged by locating the first five nodes in the gas-side within the viscous sublayer adjacent to the gas–liquid interface and expanding the rest of the grid points to the channel centerline using a factor of 1.04. To produce grid-independent results, numerical experiments for several grid arrangements are performed and a comparison of the local Nusselt number $Nu_x$ for a typical case is shown in Table 1. It was noted that the differences in the local Nusselt number, $Nu_x$, from computations using either $201 \times 201 \times 41$ or $101 \times 101 \times 21$ grids were always within 2%. To reduce the cost of computation, the $101 \times 101 \times 21$ grid was chosen for the subsequent computations. To check further the adequacy of the numerical scheme, computations were first carried out for the limiting case of turbulent mixed convection heat and mass transfer in a vertical wetted channel without consideration of the transport processes in the liquid film. The predicted results were compared with those of Yan [19]. Excellent agreement between present predictions and those of Yan [19] was found. In view of these validations, the present numerical algorithm and employed grid layout are adequate to obtain accurate results for practical purposes.

## 5. Results and discussion

In view of the large number of parameters and of the extreme demands of the computational task, a full parametric exploration is unrealistic. Rather, the parameters were varied systematically in order to examine the key trends in the results. In what follows, results are particularly presented for water film evaporation. In the light of practical situations, certain conditions are selected in the computations: Unsaturated moist air with relative humidity $\phi = 50\%$ at 20°C and 1 atm enters a long vertical channel, with half channel width $b = 0.04$ m, from the top by the combined action of certain external force as well as the buoyancy forces of thermal and mass diffusion. The inlet gas stream Reynolds number $Re$ is $2 \times 10^4$ or $5 \times 10^4$, the liquid flow rate $B$ is chosen to be 0.02, 0.04 or 0.08 kg m$^{-1}$ s$^{-1}$, and inlet liquid temperature $T_{\ell i}$ is 40 or 60°C.

Shown in Fig. 2 are the axial developments of the interfacial temperature and wall temperature. An overall inspection of Fig. 2 discloses that the deviation between the interfacial and wall temperatures is small, except for the results near the inlet. It is also clear that the liquid film temperature decreases with $X$ due to the evaporative

Table 1
Comparisons of local $Nu_x$ for various grid arrangements for $B = 0.08$ kg m$^{-1}$ s$^{-1}$, $T_{\ell i} = 60$°C and $Re = 2 \times 10^4$

| | $X$ | | | | | |
|---|---|---|---|---|---|---|
| $I \times J \times K$ | 1.047 | 5.259 | 10.104 | 20.10 | 40.84 | 60.0 |
| $201 \times 201 \times 41$ | 648.87 | 372.19 | 326.77 | 294.10 | 269.90 | 263.88 |
| $201 \times 101 \times 21$ | 648.64 | 372.69 | 327.30 | 294.59 | 270.52 | 264.51 |
| $101 \times 101 \times 21$ | 638.85 | 372.39 | 327.74 | 294.88 | 270.82 | 264.66 |
| $101 \times 51 \times 11$ | 641.08 | 374.91 | 329.86 | 296.80 | 272.70 | 266.57 |
| $51 \times 51 \times 11$ | 659.24 | 378.51 | 330.91 | 297.36 | 273.35 | 267.09 |

$I$: total grid points in the axial direction; $J$: total grid points in the transverse direction at the gas side; $K$: total grid points in the transverse direction at the liquid side

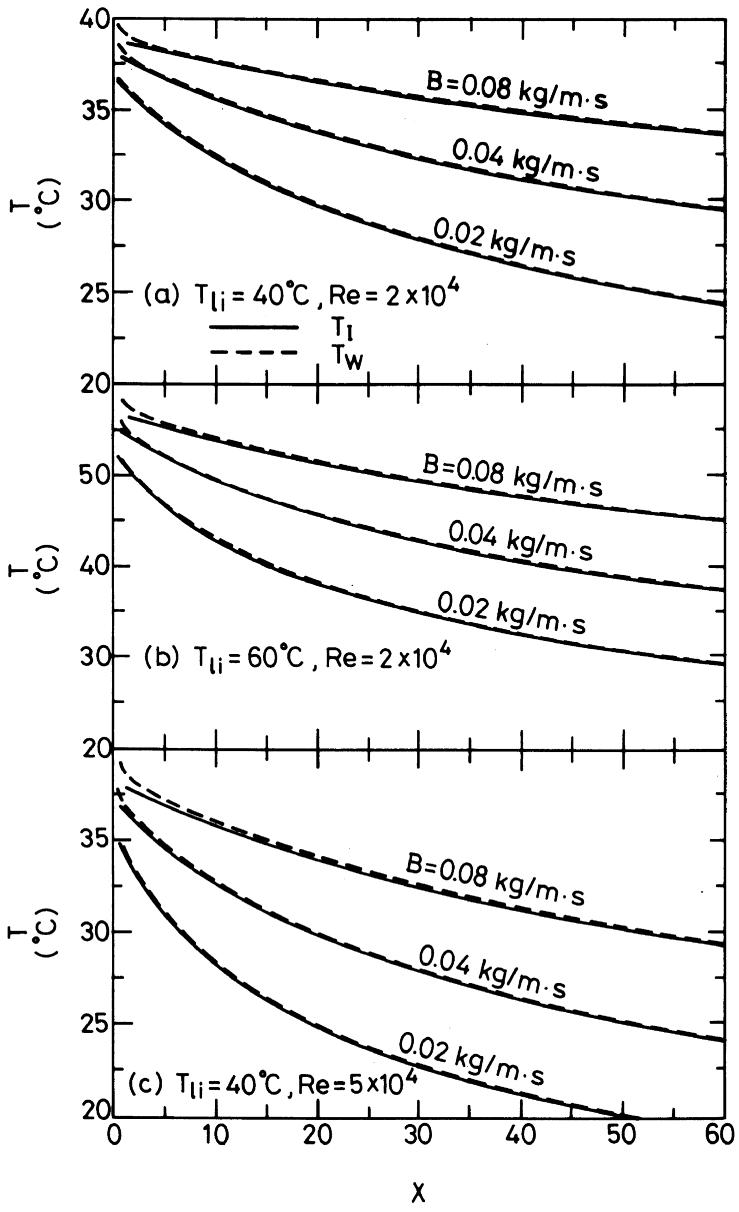


Fig. 2. Axial distributions of interfacial and wall temperatures.

cooling. This can be made plausible by noting the fact that due to film vaporization, the energy required to sustain the evaporation must largely come from the internal energy of the liquid film which then experiences a reduction in liquid film temperature. Besides, a smaller liquid film cooling (i.e. a smaller temperature drop) is experienced for a larger liquid mass flowrate. This is readily understood by realizing that the total internal energy stored in the liquid film (i.e. $Bc_p\Delta T_\ell$) is in a larger quantity for the system with a larger liquid flowrate $B$. Hence for a larger $B$, $\Delta T_\ell$ is smaller. Additionally, a larger temperature decrease results for a higher $T_{\ell i}$ by comparing the corresponding curves in Figs 2(a) and 2(b). This is a direct consequence of the larger difference in water vapor concentration between the interface and gas stream for a higher $T_{\ell i}$ which, in turn, causes larger film vaporization and temperature drop. By comparing Figs 2(a) and 2(b), it is found that a larger temperature drop is noted for a system with a higher $Re$. This confirms the general concept that for turbulent convection flow,

the heat and mass transfer is more effective for a higher $Re$. The axial distributions of the interfacial mass fraction are illustrated in Fig. 3. The water vapor concentration follows the same trend as the interfacial temperature since the thermodynamic equilibrium was assumed there. Due to the evaporative cooling of liquid film, the interfacial temperature decreases with $X$. Therefore, the corresponding mass fraction of water vapor then decreases along the channel.

To demonstrate the relative importance of the sensible and latent heat exchanges along the gas–liquid interface, the variations of local Nusselt numbers for the sensible and total heat transfer along the interface are shown in Figs 4(a) and 4(b). The total Nusselt number $Nu_x$ is the sum of latent heat Nusselt number $Nu_\ell$ and sensible heat Nusselt number $Nu_s$. The deviation between the $Nu_x$ and $Nu_s$ corresponds to the results of latent heat Nusselt number $Nu_\ell$. An overall inspection on these two plots indicates that the interfacial heat transfer due to latent heat exchange is much more effective. Regarding $Nu_s$-curves, a smaller $Nu_s$ is found for a higher $T_{\ell i}$, except for results at the downstream. This is a direct consequence of the larger blowing effect (evaporating effect) and opposing buoyancy effect for systems having a higher $T_{\ell i}$. Besides, a smaller $Nu_s$ is experienced for a larger liquid flowrate $B$. This can be made plausible by noting that a smaller

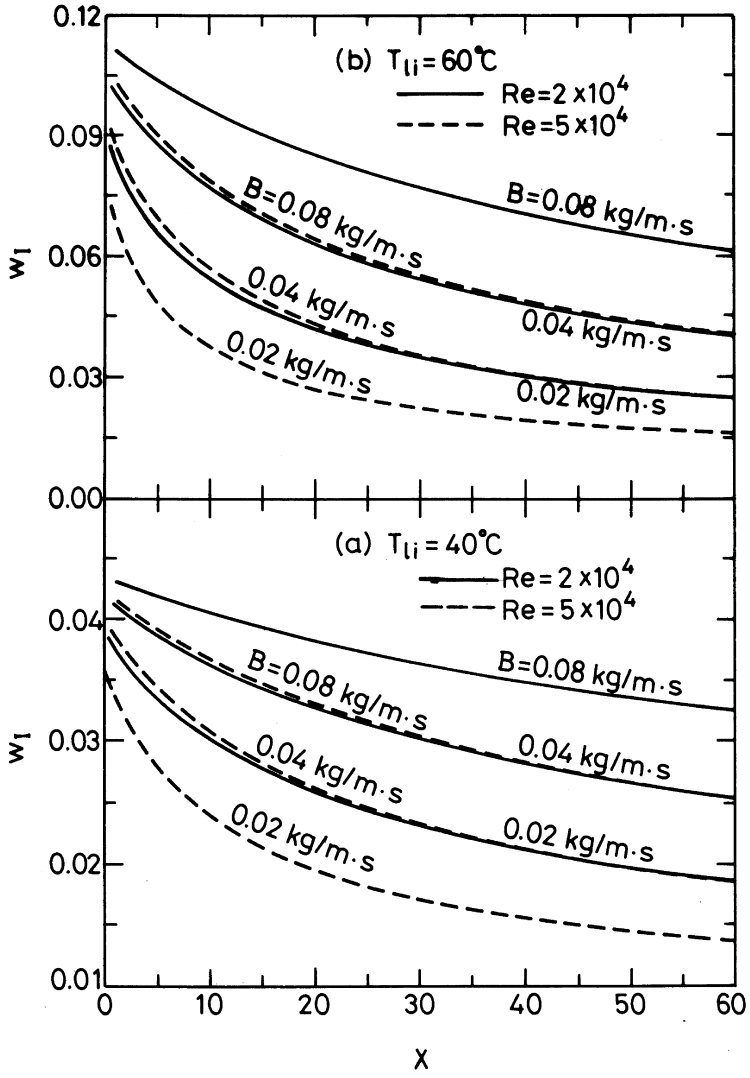


Fig. 3. Axial distributions of mass fraction of water vapor at the gas–liquid interface.

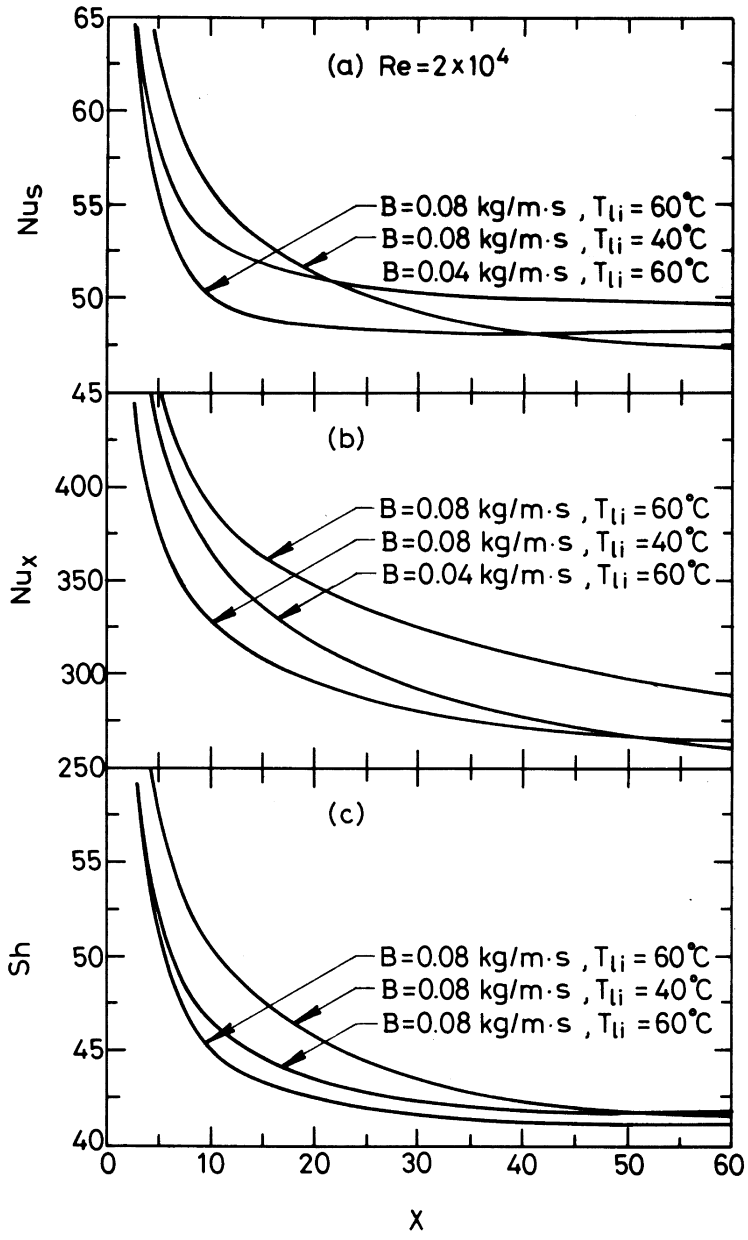


Fig. 4. Axial distributions of local $Nu_s$, $Nu_x$ and $Sh$.

liquid film cooling (i.e. a smaller temperature drop) is experienced for a larger liquid mass flowrate, which in turn, causes a greater blowing effect (evaporative effect) created by the falling liquid film for a larger $B$.

Also noted in Fig. 4(b) is that a higher $T_{fi}$ shows a larger $Nu_x$. This is brought about by the larger latent heat transfer in conjunction with the greater film vaporization for a higher $T_{fi}$. It is of interest to notice that a larger $Nu_x$ results for a larger $B$. This is again due to the larger latent heat transfer for a system with a larger $B$, i.e. a larger interfacial liquid film temperature.

The variations of local Sherwood number $Sh$ are depicted in Fig. 4(c). A larger $Sh$ results for systems with a lower $T_{fi}$ or a smaller $B$. This is due to the smaller opposing buoyancy effect for a lower $T_{fi}$ or a smaller blowing effect for a smaller $B$.

In the study of the evaporative cooling, the total temperature drop of the liquid film as it flows from the inlet

to the outlet ($X = 60.0$) is one of the important quantities. For this reason, the total temperature drop of the liquid film is presented in Fig. 5 at different conditions. For comparison purposes, the results without consideration of buoyancy effects are also included in this figure by the dashed curves. An overall inspection of Fig. 5 indicates that the buoyancy effects on the evaporative cooling is insignificant, except for the results of higher $T_{\ell i}$. It is also found that a larger liquid temperature drop is experienced for a system with a larger $T_{\ell i}$ or a smaller $B$. In addition, a larger temperature depression is found for the system with a higher Reynolds number $Re$. This confirms the general concept that for turbulent convection flow, the heat transfer is larger for a higher $Re$.

## 6. Conclusions

The characteristics of the evaporative cooling of liquid film in turbulent mixed convection channel flows have been studied. The effects of the inlet liquid temperature $T_{\ell i}$, liquid flowrate $B$ and gas stream Reynolds number $Re$ on the momentum, heat and mass transfer in the flow are investigated in detail. What follows is a brief summary of the major results:

1. The cooling of the liquid film is mainly caused by the latent heat transport associated with the vaporization of the liquid film.
2. The effects of the evaporative latent heat transfer on the cooling of the liquid film depend largely on $T_{\ell i}$ and

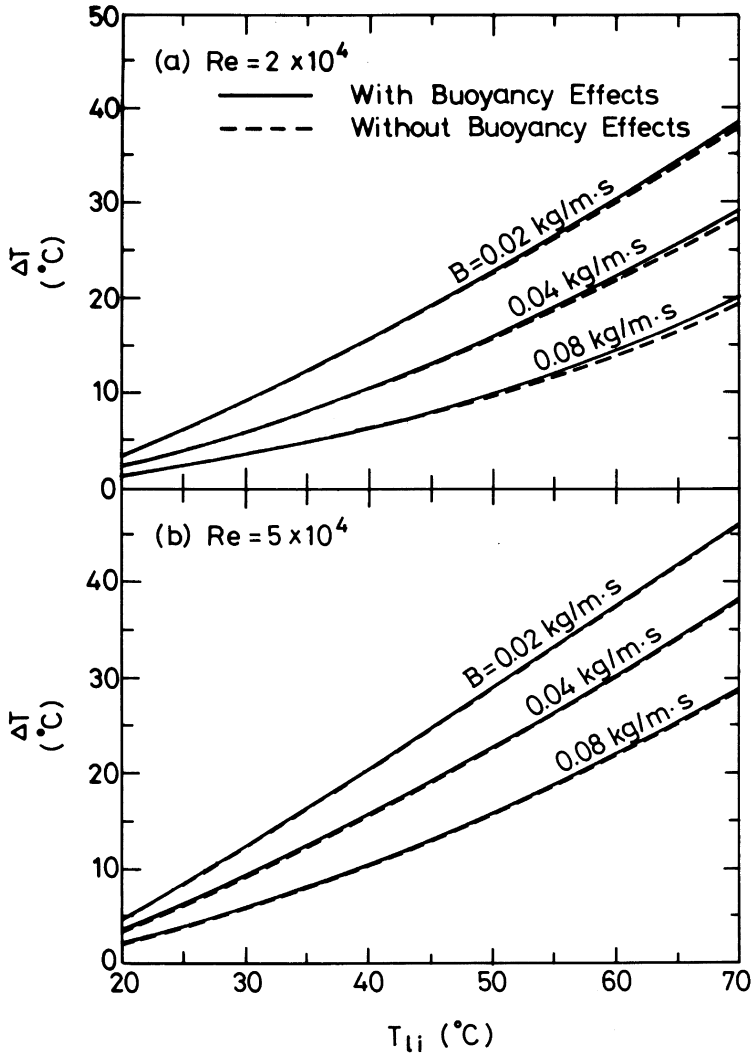


Fig. 5. Effects of liquid flow rate $B$ and inlet liquid temperature $T_{\ell i}$ on temperature drop of liquid film.

$B$. The liquid film experiences a larger temperature drop for a rise in the inlet liquid temperature $T_{\ell i}$.
3. Larger latent heat Nusselt number $Nu_{\ell}$ results for the system with a higher $T_{\ell i}$ and $B$. This is brought about by the larger latent heat transport associated with the greater film evaporation for a higher $T_{\ell i}$ and $B$.
4. A rise in liquid flowrate $B$ or a reduction in $T_{\ell i}$ causes a large $Nu_s$ or $Sh$.

## Acknowledgement

The financial support of this work by the engineering division of National Science Council, R.O.C., through the contract NSC 85-2212-E-211-004 is gratefully acknowledged.

## References

[1] Carr AD, Connor MA, Buhr HO. Velocity, temperature, and turbulence measurement in air for pipe flow with combined free and forced convection. ASME J Heat Transfer 1973;95:445–52.
[2] Conner MA, Carr AD. Heat transfer in vertical tubes under conditions of mixed free and forced convection. 6th Int Heat Transfer Conference, Toronto, Canada, 1978, 2, 43–8.
[3] Ackerman JW. Pseudoboiling heat transfer to supercritical pressure water in smooth and ribbed tubes. ASME J Heat Transfer 1970;92:490–8.
[4] Axcell BP, Hall WB. Mixed convection to air in a vertical pipe. 6th Int Heat Transfer Conference, Toronto, Canada, 1978, 2, 37–42.
[5] Easby JP. The effect of buoyancy on flow and heat transfer for a gas passing down a vertical pipe at low turbulent Reynolds number. Int J Heat Mass Transfer 1978;21:791–801.
[6] Nakajima M, Fukui K, Ueda H, Mizushinal T. Buoyancy effects on turbulent transport in combined free and forced convection between vertical parallel plates. Int J Heat Mass Transfer 1980;23:1325–36.
[7] Abdelmeguid AM, Spalding DB. Turbulent flow and heat transfer in pipe with buoyancy effects. J Fluid Mechanics 1979;94:383–400.
[8] Tanaka H, Maruyama S, Hatano S. Combined forced and natural convection heat transfer for upward flow in a uniformly heated, vertical pipe. Int J Heat Mass Transfer 1987;30:165–74.
[9] Cotton MA, Jackson JD. Vertical tube air flows in the turbulent mixed convection regime calculated using a low-Reynolds-number $k$–$\varepsilon$ model. Int J Heat Mass Transfer 1990;33:275–86.
[10] Torii S, Shimizu A, Hasegawa S, Higasa M. Laminarization of strongly heated gas flows in a circular tube (numerical analysis by means of a modified $k$–$\varepsilon$ model). JSME Int J 1990;33(II):538–47.
[11] Chow LC, Chung JN. Evaporation of water into a laminar stream of air and superheated steam. Int J Heat Mass Transfer 1983;26:373–80.
[12] Chow LC, Chung JN. Water evaporation into a turbulent stream of air, humid air or superheated steam. 21st ASME/AIChE National Heat Transfer Conference, Seattle, WA, ASME Paper No. 83-HT-2, 1983.
[13] Schroppel J, Thiele F. On the calculation of momentum, heat and mass transfer in laminar and turbulent boundary layer flows along a vaporizing liquid film. Numer Heat Transfer 1983;6:475–96.
[14] Wu CH, Davis DC, Chung JN, Chow LC. Simulation of wedge-shaped product dehydration using mixtures of superheated steam and air in laminar flow. Numer Heat Transfer 1987;11:109–23.
[15] Chandra V, Savery CW. Forced convection heat and mass transfer from a falling film to a laminar external boundary layer. Int J Heat Mass Transfer 1974;17:1549–57.
[16] Chandra V. Mass, momentum and heat transfer from a falling film to a countercurrent air stream. Ph.D. thesis, Drexel University, 1975.
[17] Lin TF, Chang CJ, Yan WM. Analysis of combined buoyancy effects of thermal and mass diffusion on laminar forced convection heat transfer in a vertical tube. ASME J Heat Transfer 1988;110:337–44.
[18] Yan WM, Tsay YL, Lin TF. Simultaneous heat and mass transfer in laminar mixed convection flows between vertical parallel plates with asymmetric heating. Int J Heat and Fluid Flow 1989;10:262–9.
[19] Yan WM. Turbulent mixed convection heat and mass transfer in a wetted channel. ASME J Heat Transfer 1995;117:229–33.
[20] Lee KT, Tsai HL, Yan WM. Mixed convection heat and mass transfer in vertical rectangular ducts. Int J Heat Mass Transfer 1997;40:1621–31.
[21] Baumann WW, Thiele F. Heat and mass transfer in two-component film evaporation in a vertical tube. Proc. 8th Int Heat Transfer Conf 1986;5:1843–8.
[22] Baumann WW, Thiele F. Heat and mass transfer in evaporating two-component liquid film flow. Int J Heat Mass Transfer 1990;33:267–73.
[23] Yan WM, Lin TF, Tsay YL. Evaporative cooling of liquid film through interfacial heat and mass transfer in a vertical channel—I. Experimental study. Int J Heat Mass Transfer 1991;34:1105–11.
[24] Yan WM, Lin TF. Evaporative cooling of liquid film through interfacial heat and mass transfer in a vertical channel—II. Numerical study. Int J Heat Mass Transfer 1991;34:1113–24.
[25] Dukler AE. Characterization, effects and modeling of the wavy gas–liquid interface. Prog heat Mass Transfer 1972;6:207–34.
[26] Kafesjan, Plank, Gerhard. Liquid flow and gas phase mass transfer in wetted wall towers. AIChE J 1961;7:463–6.
[27] Seban RA, Faghri A. Evaporation and heating with turbulent falling liquid films. ASME J Heat Transfer 1976;98:315–8.
[28] Yih SM, Liu JL. Falling liquid film with or without interfacial shear AIChE J 1983;29:903–9.
[29] Eckert ERG, Drake RM Jr. Analysis of heat and mass transfer. New York : McGraw-Hill, 1972.
[30] Bird RB, Stewart WE, Lightfoot EN. Transport phenomena. New York : Wiley, 1960.

[31] Reid RC, Prausnitz JM, Sherwood TK. The properties of gas and liquid. New York : Hemisphere/McGraw-Hill, 1977.
[32] Fujii T, Kato Y, Bihara K. Expressions of transport and thermodynamic properties of air, steam, and water. Sei San Ka Gaku Ken Kyu Jo., Report No. 66, Kyu Shu University, Kyu Shu, Japan 1977.
[33] Myong HK, Kasagi N, Hira M. Numerical prediction of turbulent pipe flow heat transfer for various Prandtl number fluids with the improved $k$–$\varepsilon$ turbulence model. JSME Int J 1989;32:613–22.
[34] Myong HK, Kasagi N. A new approach to the improvement of $k$–$\varepsilon$ turbulence model for wall bounded shear flow. JSME Int J 1990;33:63–72.
[35] Patankar SV. Numerical heat transfer and fluid flow. New York : Hemisphere/McGraw-Hill, 1980.